

Effect of Ni Doping on Electrocatalytic Hydrogen Evolution Activity of MoS₂

Congrong Wang^{1,3}, Shun Wang¹, Jianguo Lv^{1,3,*}, Yuxuan Ma¹, Gaoliang Zhou¹, Mingsheng Chen², Yongqi Wang¹, Min Zhao^{1,3,*}, Xiaoshuang Chen⁴

¹ School of Physics and Materials Engineering, Hefei Normal University, Hefei 230601, China

² School of Electronic Information and Electrical Engineering, Hefei Normal University, Hefei 230601, China

³ Universities Joint Key Laboratory of Photoelectric Detection Science and Technology in Anhui Province, Hefei 230601, China

⁴ National Laboratory for Infrared Physics, Shanghai Institute of Technical Physics, Chinese Academy of Sciences, Shanghai 200083, China

*E-mail: lvjg1@163.com (J. Lv), zhaomin@hfnu.edu.cn (M. Zhao).

Received: 7 July 2019 / Accepted: 11 October 2019 / Published: 29 October 2019

Pure MoS₂ and Ni doped MoS₂ were prepared by mean of hydrothermal method. The microstructure, surface morphology and chemical composition were investigated by X-ray diffractometer, Raman spectroscopy, FE-SEM and XPS. The diffraction peak corresponding to (002) lattice plane shifts to smaller angle when Ni atoms incorporate into MoS₂ crystal lattice. Few layer MoS₂ nanosheets with perpendicularly oriented structure appeared when MoS₂ were doped with moderate Ni. The electrocatalytic hydrogen evolution reaction of the pure MoS₂ and Ni-MoS₂ was investigated by LSV and EIS. The results indicated that the Ni-1.0-MoS₂ exhibits the best HER activities. The overpotentials at 10mA cm⁻² and the charge transfer resistance (R_{ct}) were 164 mV (vs. RHE) and 89 Ω , respectively. The Ni-1.0-MoS₂ electrocatalysts also exhibited good stability, which was significantly for potential applications in the field of electrocatalysis.

Keyword: Ni-MoS₂; Electrocatalysis; Hydrogen evolution reaction; Hydrothermal method

1. INTRODUCTION

In recent years, many serious environmental problems have been caused by fossil energy consumption and attracted the global attention {Pu, 2015 #2347;Balat, 2009 #2348}. It is necessary to develop a renewable energy to meet the needs of production and life. A lot of attempts have been carried out to look for a low-cost and clean new energy sources {Liu, 2017 #2346;Ren, 2016 #2349}. As a green, abundant, high-density fuel, hydrogen has been thought as the best energy substitutions for the

future {Ren, 2016 #2350}. It is thought that electrocatalytic water splitting is the best technique to hydrogen production {Xiong, 2018 #2351}. The hydrogen evolution reaction (HER) is the important half reaction in electrochemical water splitting, which highly rely on the electrocatalytic activity. Currently, Pt-group metals are the most advanced HER catalysts. However, insufficient reserves and high prices limit the application range of these materials for electrocatalysts. Thus, development of non-noble metal HER electrocatalysts deemed to be of great significance for future energy conversion, storage and application {Al-Mamun, 2016 #2352;Chen, 2011 #2353}. MoS₂ is one of the layered chalcogenides, which has been acted as promising alternatives for noble metals in the past few years {Zhao, 2015 #2360;Li, 2019 #2361;Liu, 2016 #2362;Huang, 2019 #2363}. However, MoS₂ in bulk form exhibits poor activity of electrocatalytic hydrogen production due to its few exposed edge active sites and poor intrinsic conductivity. Therefore, many methods have been projected to devise MoS₂ with few-layers structure and nano-size so as to increase the exposed edge active sites. In addition, regulating electronic structure by elemental doping (such as cobalt and iron) and coupling with conductive materials have also been proposed to improve electrical conductivity of MoS₂ and decrease the hydrogen adsorption energy for higher electrocatalytic HER {Deng, 2015 #2354;Xiong, 2018 #2351;Wu, 2017 #2357;Si, 2019 #2358}. However, researches involving the electrocatalytic HER on Ni doped MoS₂ have been seldom reported {Li, 2018 #2359}.

In this letter, Ni doped MoS₂ were prepared by a simple hydrothermal synthesis.

Ni doping has an significant effects on microstructure, surface topography, composition and element valence of the MoS₂. Compared to pure MoS₂, the Ni-MoS₂ exhibited preferable electrocatalytic HER performance in H₂SO₄ solution with the concentration of 0.5 M. The Ni-MoS₂ composite electrocatalysts could be easily prepared and used as a cathode materials in the field of electrocatalytic HER.

2. EXPERIMENTAL

In a typical synthesis, 14 mmol hexaammonium heptamolybdate tetrahydrate ((NH₄)₆Mo₇O₂₄·4H₂O), 60 mmol thiourea (CH₄N₂S) were put into 80 mL deionized(DI) water. Subsequently, 0.2 mmol, 1.0 mmol or 1.4 mmol nickel nitrate (Ni(NO₃)₂) were added the above-mentioned solution, which was vigorous stirred to obtain uniform solution. After that, the solution was poured into a Teflon-lined stainless steel autoclave a volume of 100 mL, which was put in oven. The autoclave was reacted at the temperature of 220° for 24 h. After reaction was completed, the sample was cooled down to room temperature. The final sample was rinsed in proper order with absolute ethanol and DI water and dried at 60 °C under vacuum. The MoS₂ with different Ni contents was named as Ni-0.2-MoS₂, Ni-1.0-MoS₂ and Ni-1.4-MoS₂, respectively. For comparison, pure MoS₂ was also prepared using similar process, but without nickel nitrate (Ni(NO₃)₂).

The crystalline structures were characterized by X-ray diffraction analysis (XRD, TD-3500) using CuK α radiation (λ = 1.5418 Å) at 40 kV and 30 mA. Raman spectra were performed by means of Raman spectroscopy (inVia-Reflex, Renishaw). The surface morphology of samples were investigated

by field emission scanning electron microscopy (FE-SEM, Hitachi S-4800). Chemical components and valence states were performed on a X-ray photoelectron spectrometer (XPS, Thermo, ESCALAB 250).

Electrochemical measurements were carried out with a three-electrode electrochemical system using an electrochemical workstation (CHI 660E). Working electrode with Ni-MoS₂ catalysts were prepared as follow: 10 mg catalysts were dispersed into 25 μL Nafion solution (5.0%, Du Pont) and 400 μL isopropyl alcohol. Then the solution was mixed thoroughly by ultrasonic treatment for 60 min and form a homogeneous ink. The ink was coated on carbon paper ($1.0 \times 1.0 \text{ cm}^2$), which was treated in an oven at 60 $^\circ\text{C}$ for 10 h. The working electrode could be obtained. For comparison, pure MoS₂ catalyst ink was also prepared as the same process as Ni-MoS₂ catalyst ink. Linear sweep voltammetry (LSV), cyclic voltammetry (CV) and chronoamperometry with a scan rate of 10 mV s^{-1} were performed in 0.5 M H₂SO₄ solution. Ag/AgCl (3 M KCl), carbon cloth and the carbon paper with various catalysts as the reference electrode, counter electrode and working electrode, respectively. The electrocatalytic stability was tested in 0.5 M H₂SO₄ solution at room temperature with the potential cycling between 0.2 and -0.4 V (vs. RHE) with a scan rate of 10 mV s^{-1} for 1000 cycles. Electrochemical impedance spectroscopy (EIS) was tested by applying a bias of 5 mV versus the Ag/AgCl electrode in a frequency range between 10⁵ and 0.1 Hz. All the final potentials were calibrated to a reversible hydrogen electrode (RHE).

3. RESULTS AND DISCUSSION

In order to understand the effect of Ni doping on crystallization of MoS₂, the XRD and Raman spectra of the Ni-MoS₂ composite powder were investigated. Fig. 1 shows the XRD spectra of MoS₂ powder with different Ni doping content. It can be seen that the pure MoS₂ sample presents three diffraction peaks at $2\theta = 14.40, 33.52$ and 58.35° , which are assigned to the (002), (101) and (110) lattice plane of the hexagonal MoS₂ phase (JCPDS 65-7025) with lattice constants of $a=3.16\text{\AA}$ and $c=12.29\text{\AA}$. For the Ni-doped MoS₂, the diffraction peak corresponding to (002) lattice plane shifts to smaller angle ($2\theta = 13.78^\circ$), which may be attributed to the larger ionic radius of Ni²⁺ ($r=0.69\text{\AA}$) than that of Mo⁴⁺ ($r=0.65\text{\AA}$) {Xu, 2017 #2342}. The diffraction peak at $2\theta = 12.21$ may be indexed to the (003) lattice plane of the ammonium nickel molybdenum oxide hydroxide phase (JCPDS 50-1414). Fig.2 exhibits the Raman spectra of pure MoS₂ and Ni-MoS₂. Two characteristic peaks E_{2g}¹ and A_{1g} of MoS₂ are observed at about 378.8 cm^{-1} and 401.7 cm^{-1} , respectively. The frequency differences (Δk) of the two Raman characteristic peaks has been used to estimate the layer number of MoS₂{Changgu, 2010 #2339}. It can be seen that the pure MoS₂ with a Δk value of 22.9 cm^{-1} indicate the formation of bilayer or trilayer MoS₂. The A_{1g} peak site red shifts and Δk value increases with the increasing of Ni doping content. The results indicate that Ni doping in MoS₂ decreasing their vibration frequency and increasing layer numbers of MoS₂. The A_{1g} mode is preferentially excited for the edge-terminated perpendicular orientation of MoS₂ nanosheets. The largest peak intensities of A_{1g} indicates the most perpendicularly oriented structure in the Ni-1.0-MoS₂ {Guo, 2017 #2340}.

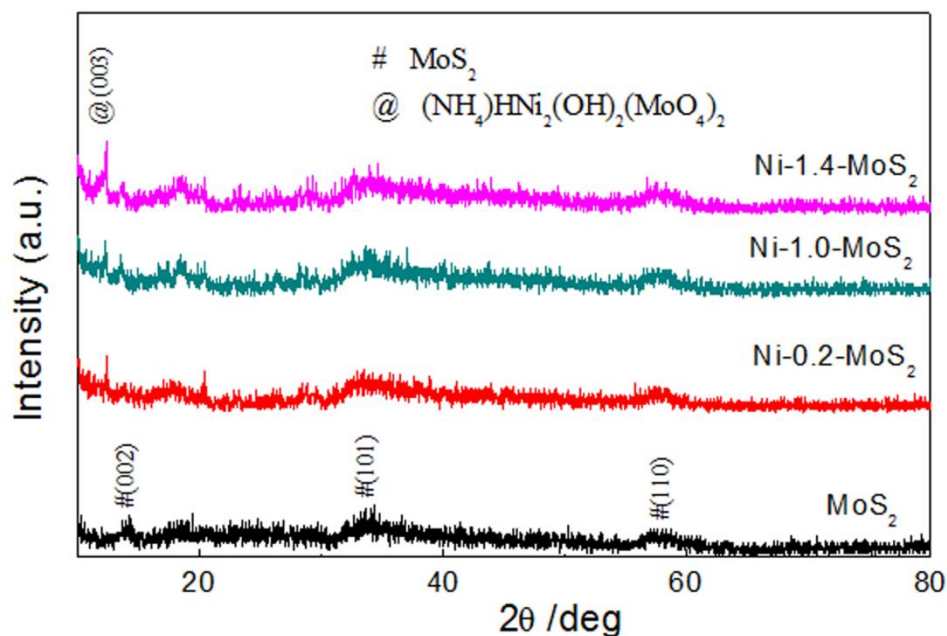


Figure 1. XRD spectra of pure MoS₂ and Ni-MoS₂.

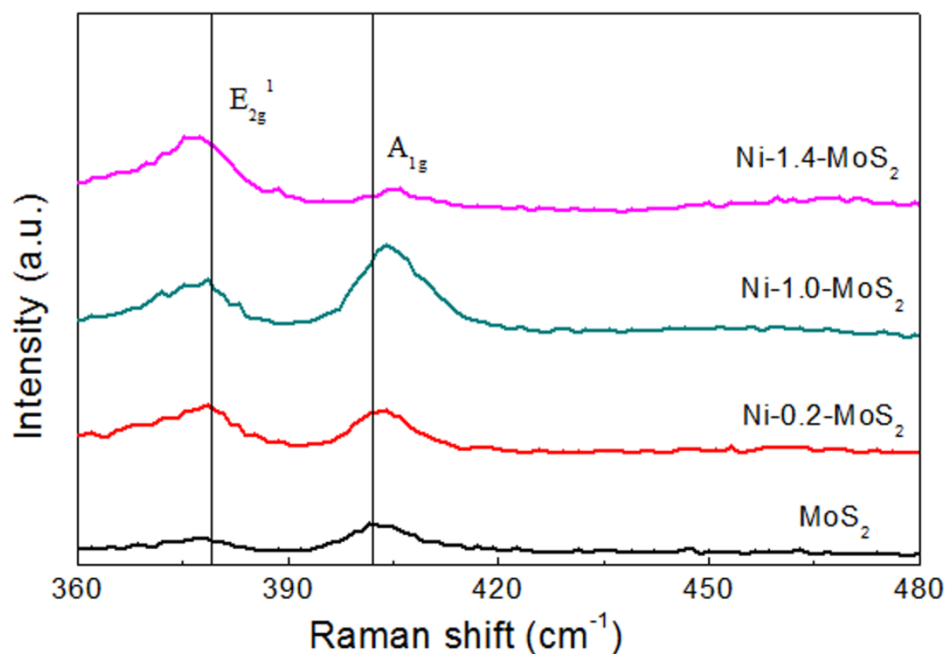


Figure 2. Raman spectra of pure MoS₂ and Ni-MoS₂.

Fig. 3 shows a typical FE-SEM images of the pure MoS₂ and Ni-MoS₂ nanosheets. It can be seen that the pure MoS₂ nanosheets are agglomerated and does not form a perpendicularly oriented structure. The perpendicularly oriented MoS₂ nanosheets appear in the Ni-0.2-MoS₂ for the first time. The Ni-0.2-MoS₂, Ni-1.0-MoS₂ have the larger specific surface area, while the Ni-1.4-MoS₂ began to lose the perpendicularly oriented feature of MoS₂ nanosheets {Guo, 2017 #2340}. Previous research results show that the edge sites of MoS₂ nanosheets are active for electrocatalytic reactions. Therefore, branched

surface morphology with high specific surface area is preferred for most electrocatalysts {Hou, 2016 #2341}.

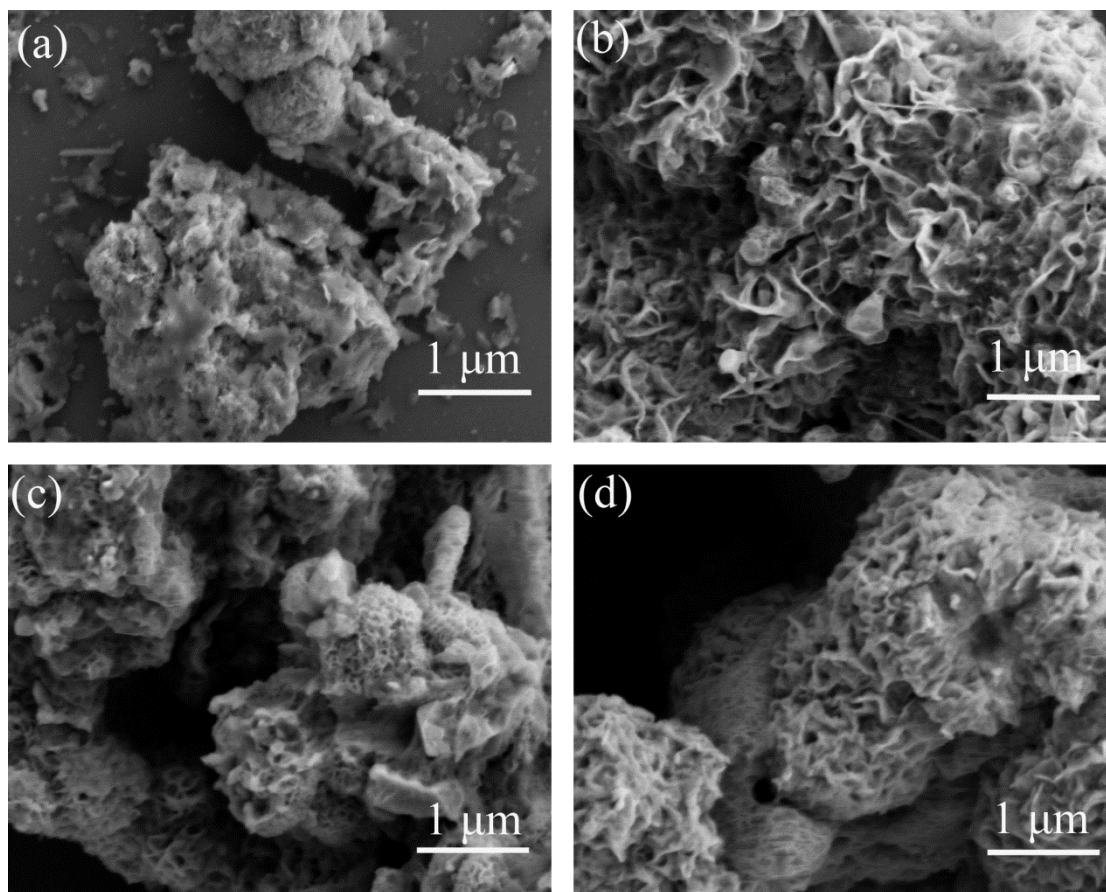


Figure 3. Typical FE-SEM images of pure MoS₂ and Ni-MoS₂ nanosheets.

In order to proclaim the chemical compositions and elemental valence states of the pure MoS₂ and Ni-MoS₂. Fig. 4a shows the high-resolution Mo3d XPS spectrum of the pure MoS₂ and Ni-1.0-MoS₂. The peaks located at 229.0 and 232.2 eV are indexed to the 3d_{5/2} and 3d_{3/2} of Mo⁴⁺ in MoS₂, respectively. The peaks located at 233.7 and 236.9 eV are related to the 3d_{5/2} and 3d_{3/2} of Mo⁶⁺, indicating the formation of (NH₄)H₂Ni(OH)₂(MoO₄)₂. The high-resolution S2p XPS spectrum of the pure MoS₂ and Ni-1.0-MoS₂ was depicted in Fig. 4b. The S2p spectrum can be deconvoluted into four and five peaks for pure MoS₂ and Ni-1.0-MoS₂, respectively. The peaks located at about 161.8 and 163.1 eV are assigned to the S2p_{3/2} and S 2p_{1/2} binding energies of S²⁻ in MoS₂ or Ni-1.0-MoS₂, respectively. The peaks located at about 164.5 and 169.1 eV and 170.1 eV are related to C-S and SO₄²⁻, respectively. The bond of C-S and S-O may originate from thiourea and residual sulfate groups on the surface of the samples {Cao, 2018 #2343}. The high-resolution Ni2p XPS spectrum for Ni-1.0-MoS₂ and the XPS spectrum with the same binding energy for the pure MoS₂ are shown in Fig. 4c. It can be seen that no peak has been observed in pure MoS₂. One peak centered at 857.4eV is related to the Ni2p_{3/2} binding energies of Ni²⁺, indicating the incorporation of Ni element in Ni-1.0-MoS₂. The high-resolution O1s XPS spectrum (Fig. 4d) is deconvoluted to two Lorentzian-Gaussian peaks for the samples. The low

energy peak at 531.8 eV corresponding to the OH⁻ groups. The high energy peak at 533.6 eV may be attributed to oxygen defects. The XPS results indicate that the existence of Mo, Ni and S elements in the Ni-1.0-MoS₂. The element content (at.%), Ni/Mo and Mo/S ratio of MoS₂ and Ni-1.0-MoS₂ are shown in Table 1. It can be seen that the atomic ratio of Mo to S in the pure MoS₂ is 0.50, suggesting the formation of stoichiometric MoS₂. The atomic ratio of Mo to S in the Ni-1.0-MoS₂ is 0.48, which slightly deviates from stoichiometric ratio. Ni atoms were incorporated into molybdenum sulfide lattices and form compounds of sulfur, molybdenum and nickel.

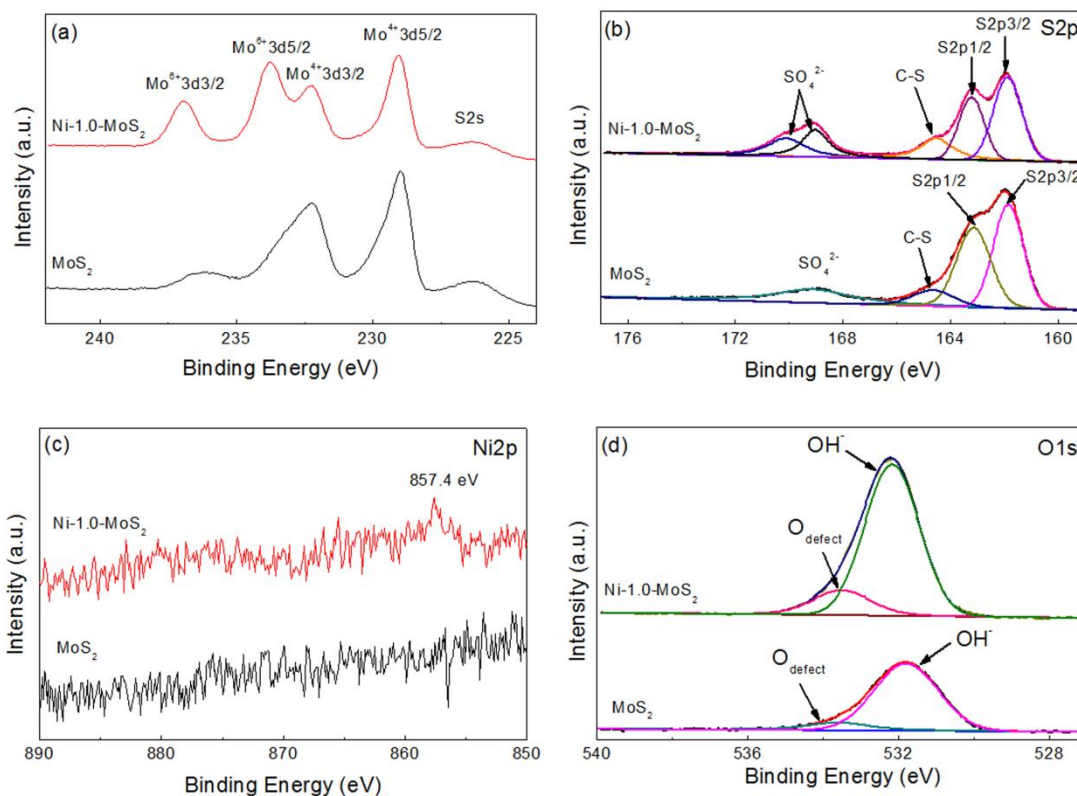


Figure 4. (a) High-resolution Mo3d, (b) high-resolution S2p (c) high-resolution Ni2p and (d) high-resolution O1s XPS spectrum of pure MoS₂ and Ni-1.0-MoS₂.

In order to clarify the role of Ni doping on the HER process, the pure MoS₂ and Ni-MoS₂ electrodes were investigated in 0.5M H₂SO₄ solution by using a typical three-electrode system. The HER activities of Pt electrode was also tested for comparisons. Cyclic voltammogram (CV) tests were firstly measured for several tens cycles before the LSV tests in order to make the catalysts stable. Fig.5a shows the LSV curves of pure MoS₂, Ni-0.2-MoS₂, Ni-1.0-MoS₂, Ni-1.4-MoS₂ and Pt with 95% iR compensation. It can be seen that the Ni doped MoS₂ present the better HER activities than that of pure MoS₂. The Ni-1.0-MoS₂ displays the overpotentials at 10mA cm⁻² of 164 mV (vs. RHE) and exhibits the best HER activities among all the Ni-MoS₂ catalysts. The result indicate that the appropriate Ni doping contents have important effect on the electronic structure of MoS₂ for high HER.

Electrochemical impedance spectroscopy (EIS) measurements were used to investigate the electrode interfacial properties and HER catalytic kinetics. EIS were performed at a given overpotential with a voltage perturbation amplitude of 5 mV in the frequency range of 100 kHz to 0.1 Hz. Fig. 5b shows the Nyquist plots for the electrodes in 0.5M H₂SO₄ solution. The charge transfer resistance (R_{ct}) can be obtained by fitting the Nyquist plot according to the equivalent circuit model {Chen, 2017 #2365}. It can be seen that the Ni-1.0-MoS₂ electrode has the smallest charge transfer resistance (R_{ct}) of 89Ω, which far less than that of the pure MoS₂ (6108Ω). It is well known that the R_{ct} is associated with the electrocatalytic kinetics at the catalyst/electrolyte interface and gives information about the reaction rate of HER {Li, 2017 #2364}. Therefore, the Ni-1.0-MoS₂ electrode has the fast charge transfer and the optimum HER kinetics.

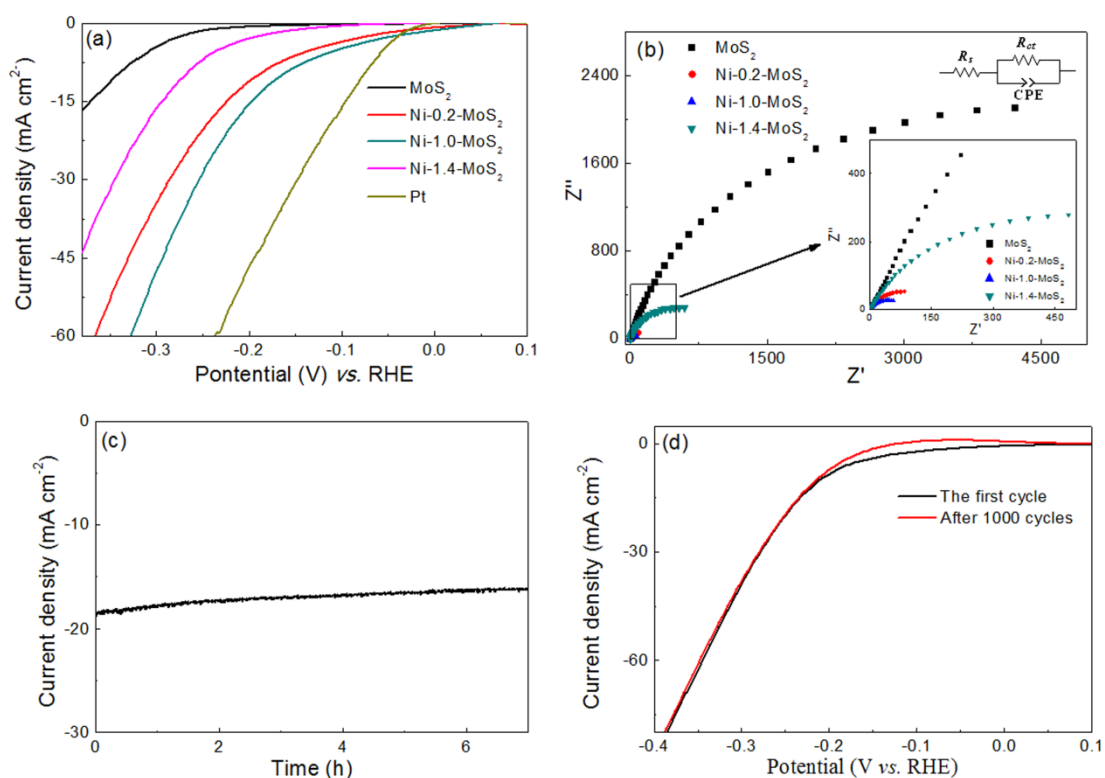


Figure 5. (a) LSV curves and (b) EIS spectra of pure MoS₂, Ni-0.2-MoS₂, Ni-1.0-MoS₂, Ni-1.4-MoS₂, (c) *I-t* curves and (d) CV cycle curves of Ni-1.0-MoS₂ electrode

In order to describe the cycling stability of the Ni-1.0-MoS₂ electrode, the curves of chronoamperometric current and CV cycles were tested. Fig. 5c presents the current-time curves of the Ni-1.0-MoS₂ electrode. It can be seen that the current density displays a negligible decrease for over 7 h when a constant potential of 0.256 V (*vs.* RHE) is applied. Fig. 5d shows the CV cycle curves of Ni-1.0-MoS₂ electrode before and after 1000 cycles. The result show that current density has little change compared to the initial value, indicating the Ni-1.0-MoS₂ electrocatalyst possesses good durability and could be used in practical electrocatalysis applications.

Table 1. The element content (at.%), Ni/Mo and Mo/S ratio of MoS₂ and Ni-1.0-MoS₂

Sample	Mo	S	Ni	Ni/Mo	Mo/S
MoS ₂	13.64	27.31	/	/	0.50
Ni-1.0-MoS ₂	16.6	34.16	0.58	0.034	0.48

4. CONCLUSION

In summary, the pure MoS₂ and Ni-MoS₂ were facilely prepared by means of a hydrothermal method. The perpendicularly oriented few layer MoS₂ nanosheets had been observed in the Ni-1.0-MoS₂, which had the larger specific surface area. In acidic medium, the overpotentials of the Ni-1.0-MoS₂ was 164 mV (vs. RHE) at 10mA cm⁻² and presented the higher electrocatalytic HER activity compared with pure MoS₂. It could be concluded from the EIS measurements that the Ni-1.0-MoS₂ had the smallest charge transfer resistance (R_{ct}) of 89Ω, which far less than that of the pure MoS₂ (6108Ω). The good durability for the Ni-1.0-MoS₂ electrocatalyst make it applied in the practical electrocatalysis.

ACKNOWLEDGEMENTS

This work was supported by National Natural Science Foundation of China (Nos. 51701001, 61804039), Academic funding projects for Top Talents in Subjects (Majors) of Universities (No. gxbjZD31), Natural Science Foundation of Anhui Higher Education Institution of China (KJ2019A0734, KJ2019A0736, KJ2017A924, KJ2017A002), Natural Science Foundation of Anhui Province (No. 1808085QE126), Foundation of Universities Joint Key Laboratory of Photoelectric Detection Science and Technology in Anhui Province (No. 2019GDTC03) and Foundation of Co-operative Innovation Research Center for Weak Signal-Detecting Materials and Devices Integration Anhui University (No. Y01008411, WRXH201703).

References

1. Z. Pu, Q. Liu, A.M. Asiri, Y. Luo, X. Sun, Y. He, *Electrochimica Acta*, 168 (2015) 133.
2. M. Balat, H. Balat, *Energy Sources, Part A: Recovery, Utilization, and Environmental Effects*, 31 (2009) 1280.
3. Y.R. Liu, X. Shang, W.K. Gao, B. Dong, J.Q. Chi, X. Li, K.L. Yan, Y.M. Chai, Y.Q. Liu, C.G. Liu, *Applied Surface Science*, 412 (2017) 138.
4. X. Ren, X. Ren, L. Pang, Y. Zhang, Q. Ma, H. Fan, S. Liu, *International Journal of Hydrogen Energy*, 41 (2016) 916.
5. Q. Xiong, X. Zhang, H. Wang, G. Liu, G. Wang, H. Zhang, H. Zhao, *Chemical Communications*, 54 (2018) 3859.
6. M. Al-Mamun, Y. Wang, P. Liu, Y.L. Zhong, X. Su, H. Zhang, H. Yang, D. Wang, Z. Tang, HuijunZhao, *J. Mater. Chem A*, 4 (2016) 18314.

7. Z. Chen, D. Cummins, B.N. Reinecke, E. Clark, M. Sunkara, T.F. Jaramillo, *ACS Nano*, 11 (2011) 4168.
8. K. Zhao, W. Gu, L. Zhao, C. Zhang, W. Peng, Y. Xian, *Electrochimica Acta*, 169 (2015) 142.
9. Y. Li, B. He, X. Liu, X. Hu, J. Huang, S. Ye, Z. Shu, Y. Wang, Z. Li, *International Journal of Hydrogen Energy*, 44 (2019) 8070.
10. Y.R. Liu, W.H. Hu, X. Li, B. Dong, X. Shang, G.Q. Han, Y.M. Chai, Y.Q. Liu, C.G. Liu, *Applied Surface Science*, 384 (2016) 51.
11. L. Huang, L. Ai, M. Wang, J. Jiang, S. Wang, *International Journal of Hydrogen Energy*, 44 (2019) 965.
12. J. Deng, H. Li, J. Xiao, Y. Tu, D. Deng, H. Yang, H. Tian, J. Li, P. Ren, X. Bao, *Energy & Environmental Science*, 8 (2015) 1594.
13. L. Wu, X. Xu, Y. Zhao, K. Zhang, Y. Sun, T. Wang, Y. Wang, W. Zhong, Y. Du, *Applied Surface Science*, 425 (2017) 470.
14. C. Si, Y. Wu, Y. Sun, Q. Liu, L. Tang, X. Zhang, J. Guo, *Electrochimica Acta*, 309 (2019) 116.
15. Y. Li, L. Wang, A. Song, M. Xia, Z. Li, G. Shao, *Electrochimica Acta*, 268 (2018) 268.
16. H. Xu, Z. Zhou, Y. Liu, Q. Liu, Z. He, S. Wang, L. Huang, H. Zhu, *Luminescence*, 32 (2017) 812.
17. L. Changgu, Y. Hugen, L.E. Brus, T.F. Heinz, H. James, R. Sunmin, *Acs Nano*, 4 (2010) 2695.
18. X. Guo, Y. Hou, R. Ren, J. Chen, *Nanoscale Research Letters*, 12 (2017) 479.
19. Y. Hou, S. Cui, Z. Wen, X. Guo, X. Feng, J. Chen, S, *Small*, 11 (2016) 5940.
20. Z.q. Cao, M.z. Wu, H.b. Hu, G.j. Liang, C.y. Zhi, *NPG Asia Materials*, 10 (2018) 670.
21. L. Chen, W. Yang, X. Liu, J. Jia, *International Journal of Hydrogen Energy*, 42 (2017) 12246.
22. R. Li, L. Yang, T. Xiong, Y. Wu, L. Cao, D. Yuan, W. Zhou, *Journal of Power Sources*, 356 (2017) 133.

© 2019 The Authors. Published by ESG (www.electrochemsci.org). This article is an open access article distributed under the terms and conditions of the Creative Commons Attribution license (<http://creativecommons.org/licenses/by/4.0/>).